Creep rupture of a linear polyethylene: 1. Rupture and pre-rupture phenomena

Teoh Swee Hin and B. W. Cherry
Department of Materials Engineering, Monash University, Clayton, Victoria, Australia 3168
(Received 21 February 1983; revised 29 July 1983)

The creep rupture behaviour of a high-density polyethylene was studied for material prepared at two different cooling rates. The rupture phenomena were dependent upon the morphology. The slow-cooled specimens had a degenerated spherulitic structure and all underwent brittle rupture. The fast-cooled specimens had a banded spherulitic structure and exhibited either ductile or brittle rupture depending upon the applied stress. Ductile creep rupture was associated with a large tertiary creep strain, with macro-necking and a stress whitening which corresponded to an increase in volumetric strain. Brittle creep rupture was associated with an absence of macro-necking, and either an absence or a small amount of tertiary creep. Stress whitening corresponding to a decrease in volumetric strain was a feature of both forms of failure above a threshold value of stress.

(Keywords: creep; morphology; necking; polyethylene; rupture; stress whitening)

INTRODUCTION

The way in which failure by creep rupture of a sample of polyethylene can occur varies widely with the conditions of stress and temperature, the molecular weight distribution, the environment and the previous thermal history of the polymer. Creep rupture has traditionally been described as occurring in either a brittle or ductile manner; however, the criteria adopted by different authors have varied so that the distinction between ductile and brittle failure is less definite than might appear at first sight. Criteria that have been adopted as characterizing ductile creep rupture include the appearance of a macro-neck in the specimen, the development of a large strain to failure, the appearance of tertiary creep, the observation of stress whitening, the appearance of the fracture surfaces and the inclination of the fracture surface to the tensile axis. The object of the present paper is to try to relate the 'pre-rupture phenomena' (macro-necking, gross axial strain, tertiary creep and stress whitening) to the failure mechanism. The factors controlling the fractographic features of the failure will be considered later.

Cooney[1] reported the results that he obtained with a range of polyethylenes of medium to high molecular weight ($MFI = 0.2$ to 3.6) and differentiated between two forms of creep rupture on the basis of the elongation to break. At high stresses and short times to failure, rupture was by a ductile mechanism involving plastic strains in excess of 100%, whereas at lower stresses and longer times to failure, rupture was by a brittle mechanism involving less than 10% plastic strain in the bulk of the material. Cooney also found that the transition to a brittle mechanism took place at much shorter times with the lower molecular weight material and with material which had been more slowly cooled from the melt. Kausch[2] observed a similar transition from a ductile to brittle rupture mode for polyethylene pipes fabricated from Hoechst GM 5010 polymer. This material had a higher molecular weight (M_w about 280 000, M_n about 12 500, $MFI = 0.1$) than that used by Cooney, and, as would have been expected from Cooney's results, the transition was delayed to even longer times.

Crissman and Zapas[3] identified three separate modes of creep rupture on the basis of whether necking of a uniaxially stressed tensile specimen took place. They worked with a moderately high molecular weight material ($M_n = 15\,000$ to 16 000, $M_w = 160\,000$) and found that at times to failure greater than about 4×10^5 s (approximately 4 days) the specimens always developed cracks and then fractured. At shorter times to failure the specimens always necked, but within this region two other modes of failure could be differentiated on the basis of whether the specimen broke almost immediately after necking (this occurred when failure took place at less than 100 s) or whether substantial drawing took place.

The process by which Crissman and Zapas prepared their specimens involved a slow cooling from the melt. Low *et al.*[4] had shown, using a fairly low molecular weight material ($M_w = 68\,000$, $M_n = 11\,400$), that, associated with the differences in microstructure between slow-cooled material and fast-cooled material, there was a difference in fracture behaviour. When tested at constant strain rate, a slow-cooled specimen gave a fracture characteristic of brittle behaviour with an absence of drawn polymer over the whole specimen, whereas a fast-cooled specimen necked and elongated to more than 100% before final rupture took place. These results mirrored those of Cooney who had shown that when he measured the transition from ductile to brittle behaviour by the change in slope of the stress–log(time to failure) relationship then the time to the transition was increased by an increase in the solidification rate.

Stress whitening is often associated with the macroscopic necking of a specimen and may therefore be regarded as a characteristic of ductile failure. However, if the stress whitening is caused by a crazing mechanism[5]

0032-3861/84/050727-08$03.00

then, since crazing normally leads to brittle fracture at low strains with the plane of fracture perpendicular to the tensile axis, the association of stress whitening with ductile failure appears contradictory. Crazing increases the volume of the material[6,7], and so a partial resolution of this problem may stem from the work of Cherry and Teoh[8] who have suggested on the basis of measurements of the change of volume accompanying some stress whitening phenomena that the origin of stress whitening need not necessarily be crazing of the material, but rather a structural change which gives rise to local variations in the refractive index. However, other stress whitening phenomena do appear to be associated with voiding and increases in volume and so in this paper it is hoped to characterize the relationships that occur between the various pre-rupture phenomena, and to show how these in turn are related to the final failure process.

EXPERIMENTAL PROCEDURE

The polymer used was high-density polyethylene (HDPE) supplied by Hoechst Australia Pty Ltd and designated GA7260 ($M_w = 6.1 \times 10^4$, $M_n = 9.5 \times 10^3$). This was the same material as had been used previously[8]. It was in powder form and was claimed by the manufacturer to contain no additives. The powder was compression moulded at 180°C between induction heated platens for 5 min, after which it was either left to cool to room temperature while still in the press, or water quenched to 70°C by circulating water at a rate of 2 gal min^{-1} through the heated platens. Specimens made using the first method of cooling were called air-cooled specimens. Specimens made using the second method were called water-quenched specimens. The air-cooled plaques took about 12 h to reach room temperature of 20°C. This corresponded to an average cooling rate of 0.22°C min^{-1}. The water-quenched plaques took about 85 s to reach 70°C. This corresponded to an average cooling rate of 78°C min^{-1}. The density of both the specimens was determined using a density gradient column. The two liquids used in the density gradient column were glycerine (density = 1.43 g cm^{-3}) and methanol (density = 0.79 g cm^{-3}). The density of the air-cooled and water-quenched specimens was 0.9730 and 0.9623 g cm^{-3} respectively. Using thin-section microscopy and small-angle light scattering (SALS), the morphology of the air-cooled specimens was found to be of a degenerated spherulitic structure with an 'X' SALS pattern which was similar to that described by Maxfield and Mandelkern[9]. The water-quenched specimens were of a banded spherulitic structure with a characteristic four-leaf SALS pattern. *Figures 1a* and *b* show the microstructure and the SALS pattern of both types of specimens.

Before test specimens were made from the HDPE plaque, the density variation across the plaque was determined. This was used as a quality control to ensure property uniformity for all the specimens. Small pieces (about 3 mm^2) were cut from the plaque along a line across its centre (a–a' in *Figure 2*). Their densities were then determined using the density gradient column. From *Figure 2*, it can be seen that the maximum density variation across the water-quenched plaque was 0.42%. This was about four times higher than that of the air-cooled plaque which had a density variation of 0.10%. The density was highest at the centre of the plaques. The probable reason for the density variation is that solidifi-

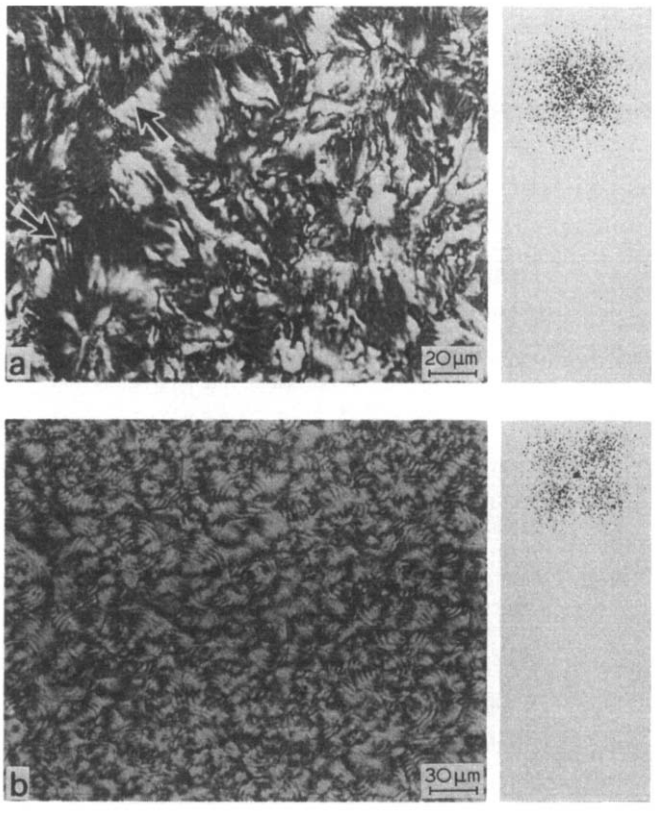

Figure 1 (a) Morphology of the air-cooled specimens viewed under crossed polars. Some obviously degenerated spherulites are indicated by arrowheads. (b) Morphology of the water-quenched specimens viewed under crossed polars. Banded spherulites with Maltese crosses can be seen

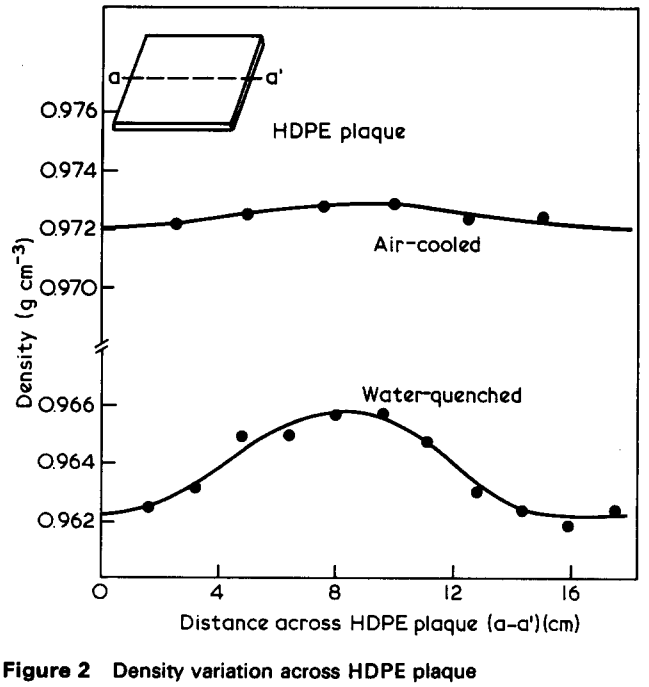

Figure 2 Density variation across HDPE plaque

cation first occurred at the edges of the plaques, since they were nearest to the cool surroundings and the poor conductivity of the HDPE further exacerbates the difference in the cooling rates between the edges and the centre of the plaque. The variation in density and thickness also resulted in some warping of the plaque. However, this was overcome by placing a weight on the plaques immediately after they were removed from the induction-heated platens.

In order to ensure consistent properties for each specimen made from the same water-quenched plaque, the centre of the plaque was discarded. Since the variation of density for the air-cooled plaque was small, the entire plaque was used for specimen making. The HDPE plaque was milled to a thickness of 2.54 ± 0.01 mm. Dumbbell-shaped specimens of gauge length 20 mm, width 5 mm were made using a polymer router. The sides of the specimen were cleaned with silicon carbide polishing paper (grade 1200) to remove machinery marks and surface scratches.

Before the polished specimens could be tested, it was necessary to determine when the density of the HDPE plaque reaches its asymptotic value since density variation changes the mechanical properties[10]. This was done by determining the density of a freshly produced plaque and plotting the density as a function of time (*Figure 3*). From *Figure 3*, it can be seen that the air-cooled HDPE reached its asymptotic value of $0.9730\,g\,cm^{-3}$ after $t_d = 2$ weeks, while the water-quenched HDPE reached its asymptotic value of $0.9625\,g\,cm^{-3}$ after $t_d = 1$ month. Hence, all the specimens were kept for a period greater than t_d before testing them.

An equipment which consists of three linear variable displacement transducers (LVDT) and a stress whitening detector was used. Two transducers were used to measure the lateral contraction while the third one measured the longitudinal extension. Their outputs were connected to x–t chart recorders. Stress whitening was detected by noting the drop in transmitted light intensity. This has been described previously by Cherry and Teoh[8].

The LVDT longitudinal strain measuring technique was calibrated using both a photographic and a clip gauge extensometer technique. In this calibration the output of the LVDT and the remote control of the camera or the clip gauge extensometer were connected to a two-channel

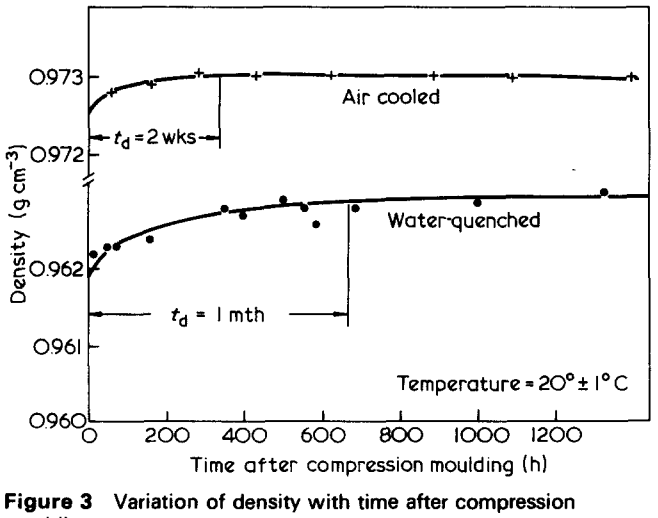

Figure 3 Variation of density with time after compression moulding

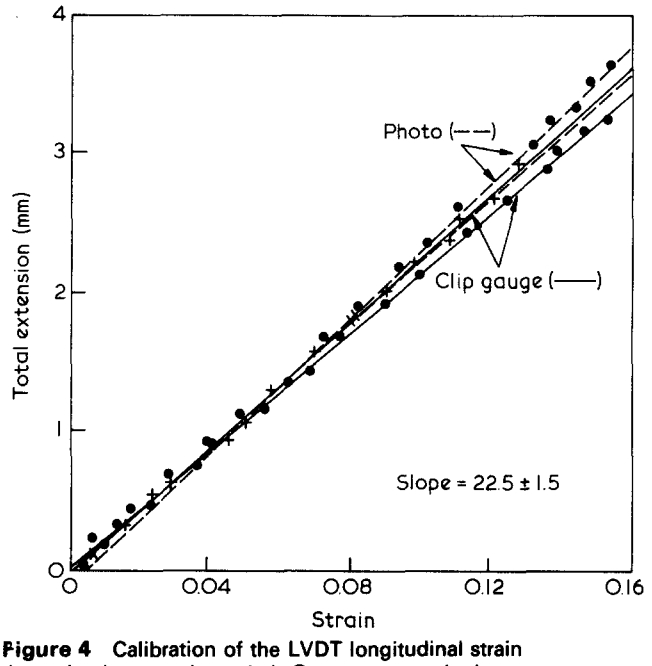

Figure 4 Calibration of the LVDT longitudinal strain determinations: x, air-cooled; ●, water-quenched

x–t chart recorder. When a photograph was taken, a tick was imprinted on the chart automatically. This helped to identify the total elongation measured by the LVDT when the photograph was taken). The strain measured from the photographs or by the extensometer was plotted against the total elongation (see *Figure 4*). A linear regression line was then plotted. It was found that the LVDT longitudinal strain measurements gave a good indication of the strain along the gauge length of the specimen, provided an initial gauge length of 22.5 ± 1.5 mm was assumed. Strains measured in this way are not always entirely reliable because the effective gauge length can change as the test proceeds and material in the shoulders of the specimen can begin to contribute to creep. However, if this were the case then it would be expected that at a given total extension (as measured by LVDT) the strain as determined from the photographic measurements would be greater than the strain as determined from the clip gauge measurements (since the photographic gauge marks are more widely separated than the clip gauge points of attachment). It can be seen from *Figure 4* that the reverse is observed and consequently it will be assumed that errors from this cause are small.

The volumetric strain (e_v) was calculated using the equation:

$$e_v = [(1 - e_x)(1 - e_y)^2 - 1] \times 100. \qquad (1a)$$

Calculation of e_v by application of (1a) depends not only upon accurate values for e_x but also upon uniform deformation in the gauge length. Any slight non-uniformity can give an artificially high value of lateral contraction strain e_y resulting in an apparent decrease in volume. In order to try to reduce errors from this source, the photographs of the specimen during creep were very carefully examined for any evidence of non-uniform lateral contraction. This was only observed in those specimens which are described as demonstrating macro-necking.

The values of the longitudinal strain (e_x) and lateral strain (e_y) were obtained from the strain–time curves generated by the outputs of the transducers on the chart

recorder. These curves were digitized and stored in a Hybrid (Analog to Digital) computer.

To reduce error due to the digitizing process and initial slip during the experiment, a plot of the lateral strain *versus* longitudinal strain was made for each volumetric measurement. A linear or a polynomial of order 3 regression line was used to fit the data points. For the majority of the water-quenched specimens which did not show macro-necking and all the air-cooled specimens, a linear regression line gave the better result. However, for the water-quenched specimens which showed macro-necking, the polynomial regression line was better. The linear correlation coefficient for both regression lines was greater than 0.998. If the linear regression line was used, the longitudinal strain in equation (1a) was replaced by:

$$e_x = e_y/v. \tag{1b}$$

The creep contraction ratio (v), defined as the ratio of the lateral and longitudinal strains, was obtained from the slope of the linear regression line. If the polynomial regression line was used, the lateral strain was replaced by:

$$e_y = ae_x + be_x^2 + ce_x^3, \tag{1c}$$

where a, b and c were obtained from the coefficients of the polynomial equation. (The choice of e_y or e_x to be the dependent or independent variable in (1b) and (1c) is purely arbitrary.)

Figure 5 shows a typical example of the variation of the lateral strain with the longitudinal strain for the two types of variation mentioned above. Curve A was fitted with a linear regression line while curve B was fitted with a polynomial regression line. For curve B, definition of the creep contraction ratio can only be made for low strain (below 14% longitudinal strain). This is illustrated by the dotted line in *Figure 5*.

The percentage drop in transmitted light intensity (D_i) due to stress whitening of the stressed specimen was calculated by using the equation:

$$D_i = (1 - I_{sp}/I_{ref}) \times 100, \tag{2a}$$

where I_{sp} = transmitted light intensity through the specimen and I_{ref} = light intensity of the lamp.

The percentage stress whitening (sw) was then defined as:

$$sw = D_i^{sw} - D_i^0, \tag{2b}$$

where D_i^0 and D_i^{sw} are the percentage drop in light intensity for a non-stress-whitened and a stress-whitened specimen, respectively.

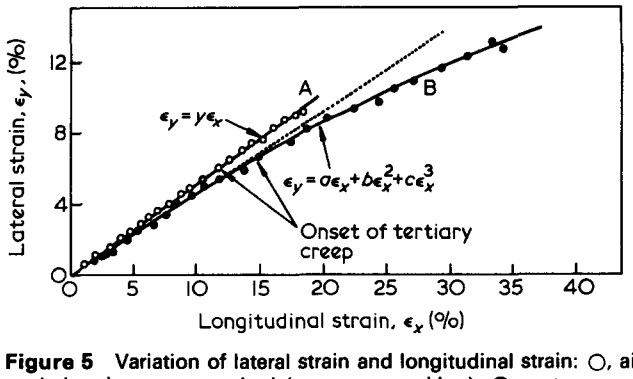

Figure 5 Variation of lateral strain and longitudinal strain: ○, air-cooled and water-quenched (no macro-necking); ●, water-quenched (macro-necking)

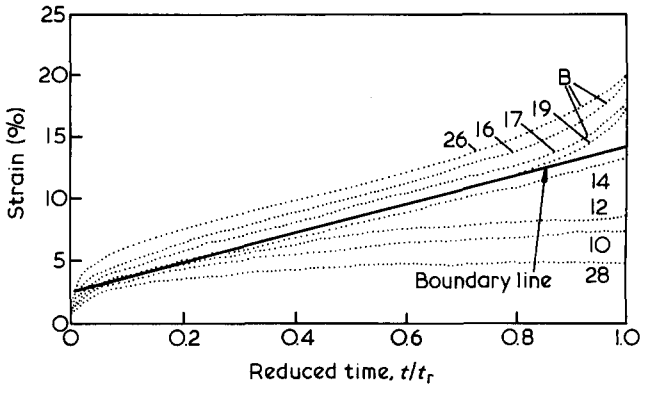

Figure 6 Strain-reduced time curves for the air-cooled specimens

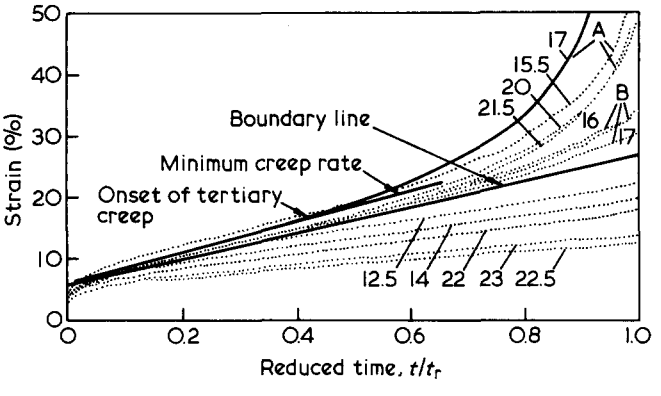

Figure 7 Strain-reduced time curves for the water-quenched specimens

Both the air-cooled and water-quenched specimens were creep rupture tested by attaching a dead weight as described previously. The applied stress was obtained by dividing the load by the initial cross-sectional area. All experiments were carried out in a constant-temperature laboratory set at 25° ± 1°C.

RESULTS

Tertiary creep

The distinction between primary, secondary and tertiary creep was made solely on the basis of the development of the creep curve. Thus the system was defined as undergoing primary creep when d^2e/dt^2 was negative, secondary creep when d^2e/dt^2 was zero and de/dt non-zero, and tertiary creep when d^2e/dt^2 was positive. No attempt was made to assign any structural basis to the descriptions adopted.

The regimes under which the various creep phenomena were demonstrated are illustrated in *Figures 6* and *7* by plotting the longitudinal strain *versus* reduced time. This technique was adopted because it enabled the tertiary creep stage to be presented graphically for the entire range of stresses. *Figures 6* and *7* show plots for the air-cooled and water-quenched specimens respectively. In *Figure 7* the strain measurements after macro-necking were inaccurate and hence were not recorded on this figure (see specimens stressed at 17, 15.5 and 20 MPa).

The reduced strain rate $\dot{e}_r$ may be defined as $de_x/d(t/t_r)$ where e_x is the longitudinal strain and t/t_r is the ratio of the

time for which the load has been applied to the total time to rupture. Results from *Figures 6* and *7* show that tertiary creep is only observed when the reduced strain rate has exceeded a certain critical value $\dot{e}_{rb}$. This value is represented by the boundary line labelled in *Figures 6* and *7*. For the air-cooled and water-quenched specimens, the value of $\dot{e}_{rb}$ is 0.19 ± 0.02 and 0.12 ± 0.02 respectively.

For specimens with a reduced strain rate below $\dot{e}_{rb}$ it may be questioned whether the process can be described as secondary creep. It is observed that the reduced strain rate decreases continuously until rupture. This indicates that below the boundary line only primary creep is exhibited.

For a reduced strain rate greater than $\dot{e}_{rb}$, two types of tertiary creep can be distinguished. They are distinguished by whether the specimen shows macro-necking or not. The two types of tertiary creep were termed Type A and Type B (see *Figures 6* and *7*). In Type A, the specimens show macro-necking and generally the total strain to rupture exceeds 35% while for Type B the total strain to rupture is below 35% and these specimens do not show macro-necking. Type A tertiary creep can also be further subdivided into Type A1 and Type A2 creep rupture on the basis that a specimen exhibiting Type A1 creep rupture cold draws after the necking process and only subsequently fractures, whereas a specimen exhibiting Type A2 rupture fractures immediately after macro-necking with no intervening cold drawing.

Volumetric variation with time

Figures 8, *9* and *10* show the variation of volumetric strain with log(time) for the air-cooled and water-quenched specimens. The onset of stress whitening and tertiary creep is indicated respectively by parallel bars (I--I) and triangles. The onset of stress whitening was taken as the point where the transmitted light intensity first started to drop[8]. The onset of tertiary creep was taken as the point where the strain–reduced time curve deviates positively from the line representing the minimum creep rate as shown in *Figure 7*.

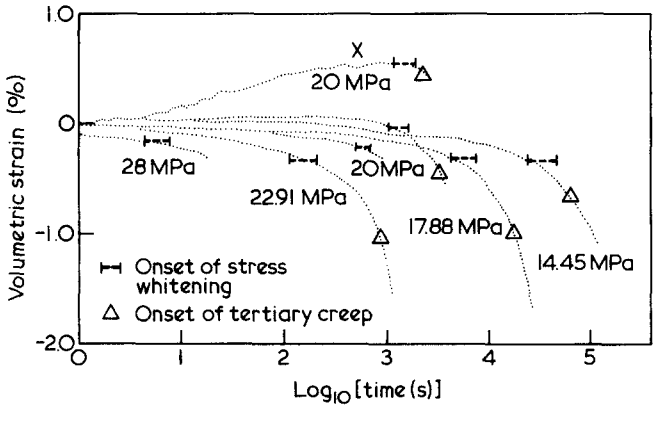

Figure 8 Variation of volumetric strain with $\log_{10}$ (time) for the air-cooled specimens

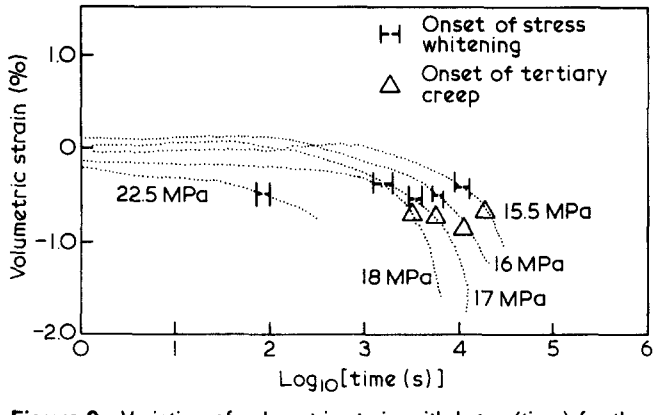

Figure 9 Variation of volumetric strain with $\log_{10}$ (time) for the water-quenched specimens that do not show macro-necking

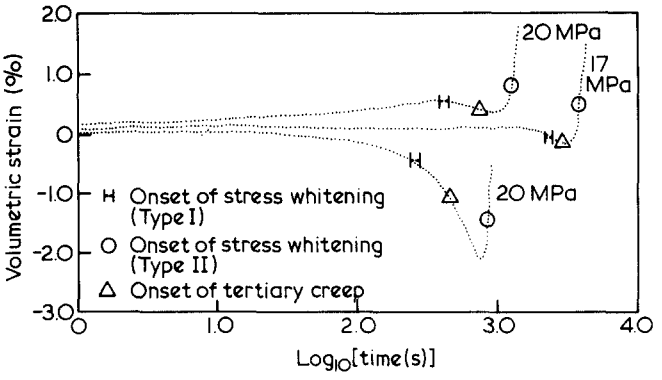

Figure 10 Variation of volumetric strain with $\log_{10}$ (time for the water-quenched specimens that showed macro-necking

The experimental scatter in the results in *Figures 8*, *9* and *10* is about $\pm 0.3\%$ and this undoubtedly conceals the initial dilatation which must result from the hydrostatic component of the applied stress. If a value of 5 GPa is assumed for the bulk modulus of polyethylene then this dilatation would be approximately 0.1%.

For all samples which demonstrated tertiary creep, the tertiary creep was associated with a decrease in volume which significantly exceeded the 0.3% limit of discrimination noted above. More surprisingly, in those samples for which stress whitening preceded tertiary creep, the stress whitening was also associated with a decrease in volume which significantly exceeded the limits of experimental error. (The major effect of an error in the 'effective initial gauge length' would be to cause a vertical shift in the results and would not invalidate this conclusion.) For the air-cooled specimens, the variation in volumetric strain with log(time) is shown in *Figure 8*. This type of variation is also typical of the water-quenched specimens which do not show macro-necking but which do exhibit stress whitening (*Figure 9*). All of the air-cooled specimens except one (*Figure 8*) had a creep contraction ratio greater than 0.5. For the one specimen where the creep contraction ratio is less than 0.5 (labelled X in *Figure 8*) the possibility that this result was caused by slip in the friction grips could not be completely eliminated. Even in this case, the onset of stress whitening was detected only after the volumetric strain started to decrease.

If the onset of stress whitening was due to microvoiding, which is a dilatational process[6,7], then one would expect stress whitening to be detected when the volumetric strain was increasing with time. This was not observed here. Nevertheless, it is inevitable that a structural change will be accompanied by microvoiding possibly in the interlamellar regions[11,12]. However, the results in *Figures 8* and *9* indicate that the volume changes resulting from such microvoiding were small compared with the changes associated with the structural transformation, and were unlikely to be the major cause of the stress whitening. This type of stress whitening, associated with a drop in the

volumetric strain, was termed Type 1 stress whitening.

For the water-quenched specimens that show macro-necking, a different type of volumetric strain variation with log(time) was observed (*Figure 10*). When the volume started to decrease, stress whitening was detected. However, towards rupture, the volumetric strain increased rapidly, indicating that the voiding process was more pronounced than the structural changes. This stress whitening phenomenon was therefore different from the one above. Hence, it is more appropriate to call this type of stress whitening, associated with a rapid increase in volumetric strain, Type II stress whitening (this is marked by circles in *Figure 10*).

Occurrence of pre-rupture phenomena

The conditions under which stress whitening and tertiary creep occur are shown diagrammatically on a graph of ln(time to rupture) *versus* applied stress in *Figures 11* and *12* for the air-cooled and water-quenched specimens respectively. These figures show that stress whitening and tertiary creep phenomena did not occur at all stress levels.

Each of the graphs can be divided into three areas. Area I is a region of low stress (below 14 MPa) where no stress whitening or tertiary creep was observed. Area II is a region of intermediate stress (between 14 and 28 MPa for the air-cooled specimens and between 14 and 22 MPa for the water-quenched specimens). Here, both stress whitening and tertiary creep were observed. Area III is a region of high stress (above 28 MPa and 22 MPa for the air-cooled and water-quenched specimens, respectively). Here, only stress whitening was detected.

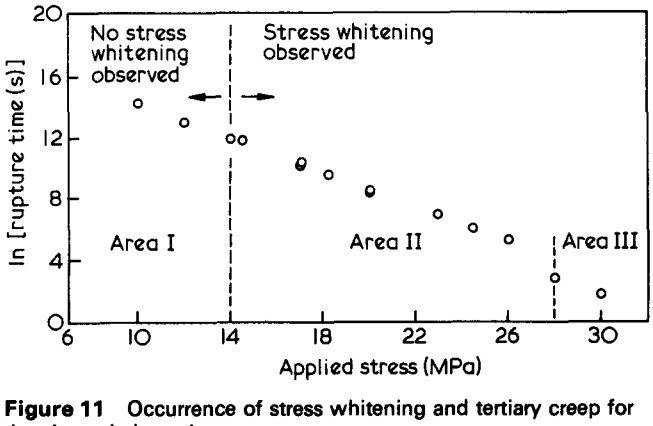

Figure 11 Occurrence of stress whitening and tertiary creep for the air-cooled specimens

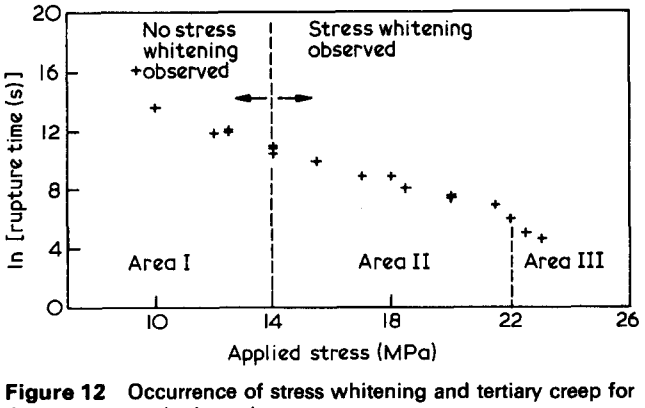

Figure 12 Occurrence of stress whitening and tertiary creep for the water-quenched specimens

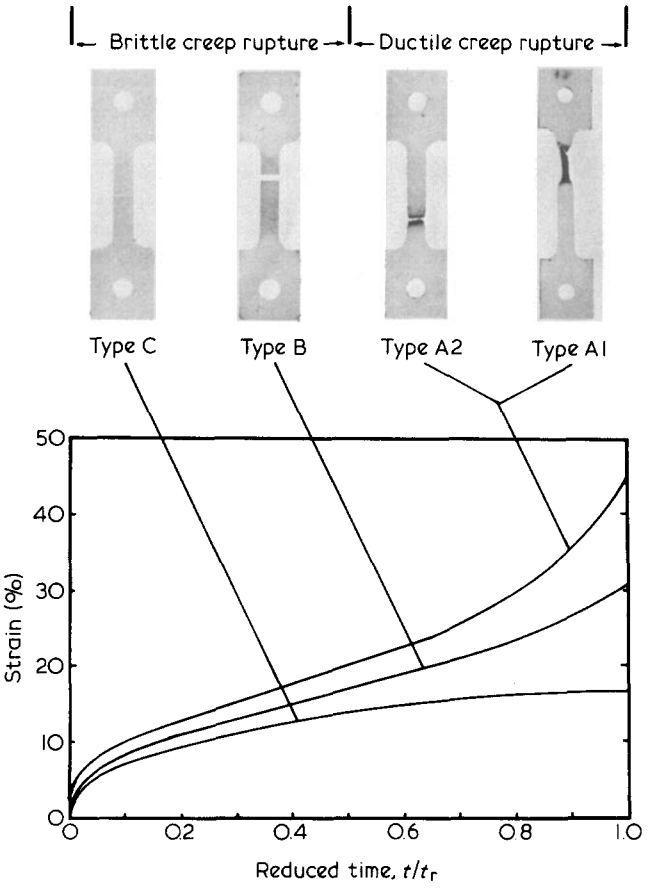

Figure 13 Schematic illustration of the four types of creep rupture behaviour in HDPE

The amount of stress whitening in Areas II and III differed. In Area II, the percentage stress whitening, calculated from the stress whitening detector outputs (equation (2b)), while the specimen was still under tension was high (greater than 10%). In Area II as well, the amount of stress whitening for the water-quenched specimens was generally higher than that for the air-cooled specimens. Values as high as 30% stress whitening had been recorded for the water-quenched specimens.

In Area III, both the air-cooled and water-quenched specimens exhibited only a small amount (less than 2%) of stress whitening. On examining the fractured specimens, it was found that the stress whitening had disappeared.

All the air-cooled specimens in Area II (*Figure 11*) demonstrated a Type B tertiary creep, that is they showed no macro-necking. The water-quenched specimens (*Figure 12*) exhibited both types of tertiary creep, that is, some of them exhibited macro-necking, whilst others showed no such macro-necking and only a moderate strain to failure.

Rupture phenomena

The appearance of typical samples of failure by creep rupture are shown in *Figure 13* and from this it may be seen that creep rupture in high-density polyethylene may take at least four separate forms which may be differentiated on the basis of the amount of tertiary creep, necking and cold drawing which take place during the failure process. Brittle creep rupture in which the plane of fracture is perpendicular to the tensile axis, in which there is a low (less than 35% in this work) strain to failure and no macro-necking, is further classified as Type C or Type B

creep rupture dependent upon whether tertiary creep is a feature of the failure process. Specimens which rupture at a low strain (typically below 13% longitudinal strain) and show no tertiary creep are classified as Type C failures, whereas specimens which demonstrate some tertiary creep but otherwise behave in a brittle manner are classified as Type B creep rupture failures.

Ductile creep rupture is associated with a large strain to failure (greater than 35% in this work) associated with considerable tertiary creep and development of macro-necking. However this ductile creep rupture cannot be identified precisely with the 'large strain to fracture, Type II' creep rupture defined by Crissman and Zapas[3] or with the 'neck formation followed by instantaneous fracture' type of creep rupture defined by Gedde and Jansson[13,14] and Gedde *et al.*[15] This is because the above authors made no clear distinction between those specimens that exhibit macro-necking and cold-drawing followed by instantaneous fracture, and those that do not show cold-drawing but exhibit macro-necking and then instantaneous fracture. In the present work the former is called Type A1 creep rupture while the latter is called Type A2. If one were to adopt the definition of Crissman and Zapas, Types A1 and A2 creep rupture are both regarded as the same since both show large strain to fracture. Similarly, the definition of Gedde and Jansson[13,14] makes no distinction between Types A1 and A2 creep rupture. At this stage, it is not apparent why Types A1 and A2 are exhibited by specimens that show the same type of tertiary creep. This will be a topic of discussion in a subsequent paper.

For Types A1 and A2 creep rupture, just before macro-necking, stress whitening of Type II (stress whitening that corresponds to an increase in volumetric strain) was seen either as distinct slip bands or localized whitened regions without slip bands. Some examples of this slip band formation for Type A1 creep rupture cannot be defined properly due to the cold-drawing of the specimen. The plane of the fracture surface for Type A2 is approximately a plane perpendicular to the tensile axis but has a more jagged appearance than that demonstrated by Type B or Type C creep rupture.

To illustrate the relationship of creep rupture types to morphology, rupture time and applied stress, the types of creep rupture exhibited by the air-cooled and water-quenched specimens are plotted on a ln(rupture time) *versus* applied stress graph. (The choice of the axes follows that of Crissman and Zapas[3].) *Figure 14* shows such a plot. (The left-hand ln(rupture time) axis is for the water-quenched specimens while the right-hand ln(rupture time) axis is for the air-cooled specimens.) Different symbols are used to represent the different types of creep rupture. The division of the applied stress into three areas is the same as those used in the study of the occurrence of pre-rupture phenomena.

For the air-cooled and the water-quenched specimens, Type C brittle creep rupture was observed in Area I and III (that is in the low- and high-stress regions). The air-cooled specimens in Area II (intermediate-stress region) showed only Type B brittle creep rupture. Neither Type A1 nor Type A2 ductile creep rupture was exhibited by the air-cooled specimens. However, for the water-quenched specimens in Area II, three types (A1, A2 and B) of creep rupture were observed. At present, there are no factors conclusively explaining this scatter of the various types of creep rupture in Area II for the water-quenched specimens. One possible factor is the large variation in the density of specimens. Such a variation could change the lamellar thickness of the spherulites, and hence may change the brittle–ductile transition of the polymer[16].

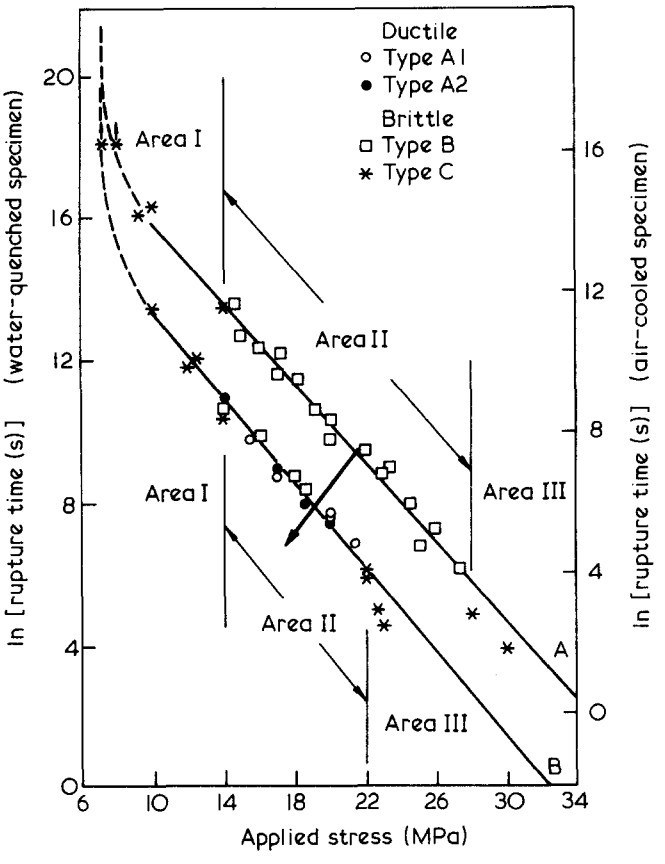

Figure 14 Variation of ln(rupture time) and applied stress for the (a) air-cooled specimens and (b) water-quenched specimens. Large arrow indicates direction of increasing cooling rate

It is interesting to note in *Figure 14* that no direct relationship exists between the types of creep rupture and the rupture time. This is in agreement with the results presented by Gedde and Jansson[13]. They have also shown that, for the same stress level, the rupture time increases with molecular weight. The molecular weight can be related to the morphology of the specimen[9]. The results in *Figure 14* indicate that, for the same stress level, the rupture time is longer for the air-cooled specimens than for the water-quenched specimens. This indicates that the type of creep rupture exhibited by a specimen is dependent on the morphology, which is in turn a function of molecular weight and crystallization conditions.

The creep rupture behaviour of the air-cooled and water-quenched specimens showed that one can obtain specimens that exhibit entirely brittle behaviour for all stress levels by decreasing the cooling rate to a very low value of about 0.22°C min^{-1}. It may be possible that one can obtain specimens that show ductile behaviour for the majority of the stress levels by increasing the cooling rate to a very high value (indicated by the large arrowhead in *Figure 14*).

CONCLUSIONS

Ductile creep rupture is related to a large extent of tertiary creep where the longitudinal strain exceeds 35% (Type A tertiary creep) and a stress whitening of Type II where the

stress whitening corresponds to a rapid increase in volumetric strain. Brittle creep rupture is related to a total absence or a small extent of tertiary creep, with a longitudinal strain of less than 35% (Type B tertiary creep). The creep rupture phenomena were not affected by Type I stress whitening since this occurred for both ductile and brittle creep rupture specimens.

For a degenerated spherulitic material (air-cooled specimens) only brittle creep rupture was observed, for all stress levels. However, for a banded spherulitic material (water-quenched specimens) at high (greater than 22 MPa and low (less than 14 MPa) stresses only brittle creep rupture was observed. At intermediate stress levels (between 14 and 22 MPa) both brittle and ductile creep rupture were observed.

The creep rupture time was independent of the types of creep rupture but dependent on the morphology of the polymer. For the same stress level a degenerated spherulitic material gave longer rupture time than a banded spherulitic material.

REFERENCES

1 Cooney, J. L. *Appl. Polym. Sci.* 1964, **8**, 1889
2 Kausch, H. H. 'Polymer Fracture', Springer-Verlag, New York, 1978
3 Crissman, J. M. and Zapas, L. *J. Polym. Eng. Sci.* 1979, **19**, 99
4 Low, A., Veseley, D., Allan, P. and Bevis, M. *J. Mater. Sci.* 1978, **13**, 711
5 Kambour, R. P. *J. Polym. Sci., Macromol. Rev.* 1973, **7**, 1
6 Bucknall, C. B. and Clayton, D. *J. Mater. Sci.* 1972, **7**, 202
7 Bucknall, C. B. and Clayton, D. *J. Mater. Sci.* 1972, **7**, 1443
8 Cherry, B. W. and Teoh, S. H. *Polymer* 1981, **22**, 1610
9 Maxfield, J. and Mandelkern, L. *Macromolecules* 1977, **10**, 1141
10 Margolies, A. F. *S.P.E. J.* 1971, **27**, 44
11 Hashimoto, T., Nagatoshi, K., Todo, A. and Kawai, H. *Polymer* 1976, **17**, 1073
12 Hashimoto, T., Nagatoshi, K., Todo, A. and Kawai, H. *Polymer* 1976, **17**, 1075
13 Gedde, U. W. and Jansson, J. F. *Polym. Eng. Sci.* 1979, **19**, 77
14 Gedde, U. W. and Jansson, J. F. *Polym. Eng. Sci.* 1980, **20**, 579
15 Gedde, U. W., Terselius, B. and Jansson, J. F. *Polym. Eng. Sci.* 1980, **20**, 732
16 Philips, P. J. and Patel, J. *Polym. Eng. Sci.* 1978, **18**, 943

'POLYMERS IN A MARINE ENVIRONMENT'

International Conference: London 31 October–2 November 1984

This conference, organised by the Polymer Physics Group of The Institute of Physics and The Royal Society of Chemistry in collaboration with The Institute of Marine Engineers, aims to bring together practical and fundamental work relevant to marine applications of polymers.

Papers relating to any use of plastics or rubbers under marine conditions will be considered and areas of interest include such topics as:

diffusion, swelling and compatible liquids
effects of water absorption
adhesion
corrosion and ageing
impact resistance and vibration isolation
electrostatic charge build-up
specialised materials
naval applications or designs
factors affecting life
practical problems

and such applications as:

inflatable or other craft
fixed or floating structures
moorings and ropes
fenders and mountings
cables and tubes
pipes and seals
paints and coatings.

For more information contact
Dr. G. J. Lake
MRPRA, Brickendonbury, Hertford SG13 8NL, UK.